Probing structural disorder in $(1-x)PbMg_{1/3}Nb_{2/3}O_3-xPbTiO_3$ single crystals by x-ray photoelectron spectroscopy

2005 J. Phys.: Condens. Matter 17 6737

(http://iopscience.iop.org/0953-8984/17/42/012)

INSTITUTE OF PHYSICS PUBLISHING JOURNAL OF PHYSICS: CONDENSED MATTER

J. Phys.: Condens. Matter **17** (2005) 6737–6749 doi:10.1088/0953-8984/17/42/012

Probing structural disorder in $(1-x)PbMg_{1/3}Nb_{2/3}O_3$–$xPbTiO_3$ single crystals by x-ray photoelectron spectroscopy

A Kania, E Talik, M Kruczek and A Słodczyk

A Chełkowski Institute of Physics, University of Silesia, ulica Uniwersytecka 4, Pl 40-007 Katowice, Poland

Received 29 April 2005, in final form 12 July 2005
Published 7 October 2005
Online at stacks.iop.org/JPhysCM/17/6737

Abstract

The $(1-x)PbMg_{1/3}Nb_{2/3}O_3$–$xPbTiO_3$ ($(1-x)$PMN–xPT) single crystals with x equal to 0, 0.22, 0.28, 0.32, 0.37, 0.47, 0.69 and 1 were studied by x-ray diffraction and x-ray photoelectron spectroscopy. X-ray diffraction results reveal that with increase of Ti content the crystal symmetry changes from pseudo-cubic, characteristic for $PbMg_{1/3}Nb_{2/3}O_3$ (PMN), to rhombohedral, then to monoclinic at the vicinity of the morphotropic phase boundary (MPB) region and finally to tetragonal, specific for $PbTiO_3$ (PT). High-resolution core level spectra of the Pb 4f, O 1s, Nb 3d and Ti 2p states show that the bulk of the $(1-x)$PMN–xPT crystals, except $PbTiO_3$ where Pb^{2+} and Pb^{4+} were detected, is characterized by only one chemical state for each element. However, in the case of the Pb and O spectra, apart from the main lines attributed to the lattice states, the satellite lines related to the surface states were also observed. The evolution of the lattice components of all core level spectra points to regular concentration dependence of the full width at half maximum (FWHM). With the rise of the Ti content the FWHMs increase and reach maxima for the MPB region, then decrease and achieve the smallest values for the pure PT. This characteristic FWHM behaviour points to disorder as an origin of the core level line broadening and it is discussed within the framework of the random field model. The FWHM of the Bragg's reflections show similar concentration behaviour which confirms the existence of the highest structural disorder in $(1-x)$PMN–xPT system near the MPB.

1. Introduction

The solid solutions formed between the relaxor ferroelectric $PbMg_{1/3}Nb_{2/3}O_3$ (PMN) or $PbZn_{1/3}Nb_{2/3}O_3$ (PZN) and ferroelectric $PbTiO_3$ (PT), i.e. $(1-x)$PMN–xPT or PMN–PT and $(1-x)$PZN–xPT or PZN–PT, have recently attracted much attention from the fundamental and application points of view. They exhibit a great variety of physical phenomena and

excellent electromechanical properties [1–3]. For compositions close to the morphotropic phase boundary (MPB) their electromechanical coupling factors, piezoelectric constants, piezoelectric strains reach the highest values yet reported [2, 3]. Hence, these materials can revolutionize a lot of devices in medicine, telecommunication and high-technology and military industries. In comparison to the classical piezoelectric material $PbZr_{1-x}Ti_xO_3$ (PZT) one component of the PMN–PT and PZN–PT solid solutions is a relaxor. Structural disorder is essential in the appearance of relaxor behaviour [1]. Therefore, one can expect that disorder may play a main role in so-called giant piezoelectricity.

Despite intensive investigations, the PMN–PT solid solutions require more systematic studies since many of their properties still remain unclear. Lead magnesium niobate $PbMg_{1/3}Nb_{2/3}O_3$ belongs to the family of $PbB'_{1-x}B''_xO_3$ perovskites and is the classical relaxor [1]. Its exceptional properties are associated with two types of structural disorder. The first one is related to random distribution of the Nb and Mg ions in the B sublattice while the second originates from disordered ion displacements. Diffraction studies showed that PMN possesses cubic symmetry with the $Pm\bar{3}m$ space group in the entire temperature range [4]. However, x-ray [5–7], neutron [8, 9], TEM [10, 11], EXAFS [12] and NMR [13] studies pointed to the presence of nanoregions with local symmetry different from $Pm\bar{3}m$. These nanoregions exhibit translational symmetry. One type of these nanoregions is related to the 1:1 order in the B-ion sublattice. According to the postulates of the charged balanced random layer model [10, 11], describing the best arrangement of the B ions, the B″ columns are exclusively occupied by Nb^{5+}, while B′ contain randomly distributed Mg^{2+} and Nb^{5+} in the ratio 2:1, which leads to the formula $Pb[(Mg_{2/3}Nb_{1/3})_{1/2}Nb_{1/2}]O_3$. Hence, the PMN consists of ordered nanoregions surrounded by a disordered matrix. The former are built of alternating Nb-rich layers with the average valence about 5+ and Nb-poor ones with the average valence about 3+, while the latter is characterized by random distribution of the B-site cations. In consequence there is ion-site disorder and each ion may exist in different chemical surrounding [13]. The charge balanced random layer model leads to the appearance of 1:1 ordered nanoregions with the $Fm\bar{3}m$ space group. Apart from these $Fm\bar{3}m$ chemically ordered clusters another kind of local symmetry appears in PMN. On cooling, at the so-called Burns temperature T_d about 620 K, the nucleation of polar nanoregions (PNRs) starts [8, 14, 15]. The PNRs are the consequence of the correlated ion off-centre displacements. B-site ions are shifted along the [111] direction about 0.18 Å, while shifts of Pb exhibit a spherically symmetric distribution with a mean diameter about 0.33–0.4 Å [15–17]. Hence each ion in the unit cell can occupy a large number of equivalent off-centre positions. At high temperature, ion displacements in every unit cell are independent of each another. When the temperature decreases, the correlations between ion shifts lead to the appearance of polar nanoregions with the rhombohedral $R3m$ symmetry. The presence of polar and 1:1 ordered nanoregions unambiguously shows that the cubic $Pm\bar{3}m$ symmetry is only an average. Therefore, PMN belongs to a class of highly disordered and inhomogeneous materials and very often is compared to dipolar glasses, especially to the spherical vector glass according to the so-called spherical random bond–random field model [18].

Without applying an electric field, long-ranged polar order is never achieved in PMN [19]. However, it is possible to induce in PMN a transition from the cubic paraelectric to the rhombohedral or monoclinic, or tetragonal ferroelectric phase by adding to PMN the ferroelectric $PbTiO_3$ (PT), which is observed in $(1-x)$PMN–xPT solid solutions. The Ti^{4+} ions, which also occupy the B site, enhance development of the long-range polar order [20]. For the Ti content from approximately 0.1 up to 0.3 relaxor behaviour is still observed, and according to the phase diagram [21] this region can be well described using rhombohedral symmetry with the $R3m$ space group. For a Ti content higher than 0.4, like in pure PT,

the normal phase transition from the cubic paraelectric phase to the ferroelectric tetragonal ($P4mm$) phase is observed. Between 0.3 and 0.4 of Ti content a very interesting region of the morphotropic phase boundary is observed. The MPB separates the rhombohedral relaxor and the tetragonal ferroelectric sides of the $(1-x)$PMN–xPT solid solutions. In the vicinity of the MPB monoclinic symmetry with the Pm space group [21, 22] was detected. In some papers the existence of a secondary phase of rhombohedral, tetragonal or even orthorhombic symmetry was also shown [21]. For materials from the MPB these different crystal structures are energetically close to each other and even a small external electric field may induce a transition between them, which seems to play an essential role in the mechanism of the appearance of giant piezoelectricity [23, 24].

The aim of this paper is a systematic high-resolution x-ray photoelectron spectroscopy (XPS) study of $(1-x)PbMg_{1/3}Nb_{2/3}O_3$–$xPbTiO_3$ single crystals with Ti content covering the whole concentration range. The core-level spectra were investigated. Because of its sensitivity to chemical surroundings, XPS spectroscopy is very useful for the characterization of the chemical environment of an element, especially in the case of disordered materials [25–28]. As stated in [26]: 'core-level x-ray photoelectron spectroscopy probes the local potentials at lattice sites in a solid and so should be able to provide information on both the conditionally averaged site potentials in a disordered alloy and fluctuations about those averages'. Up to now the systematic XPS studies of PMN–PT solid solutions have not been reported and only a few papers concerned mainly with pure PMN are available [29–31].

XPS results were compared with x-ray powder diffraction data obtained for the same single crystals.

2. Experiment

$(1-x)PbMg_{1/3}Nb_{2/3}O_3$–$xPbTiO_3$ single crystals with x equal to 0, 0.09, 0.22, 0.28, 0.32, 0.35, 0.37, 0.47, 0.69 and 1 were grown by a flux method. The PbO–Pb_3O_4–B_2O_3 system was used as a solvent. The crystallization processes were carried out in the temperature range from 1080 to 900 °C with a cooling rate of about 1°C h^{-1}. At 900 °C the solvent was poured out and the Pt crucible with the grown crystals was slowly cooled to room temperature. By etching in hot water solution of acetic acid the remains of the solvent were removed; in addition, the crystals were softly separated from the platinum crucible. Yellow, transparent, rectangular shaped single crystals of size up to $6 \times 6 \times 3$ mm^3 were obtained. The crystal compositions indicated above were determined by energy dispersion x-ray spectroscopy (EDS) using a JSM-5410 scanning electron microscope. Further technological details are given in [32].

The powder samples were obtained by crushing and milling single crystals. X-ray diffraction measurements were performed using a high-resolution Siemens D5000 diffractometer (θ–θ geometry, filtered Cu Kα radiation, $V = 40$ kV and $I = 30$ mA). The full spectrum of each sample was recorded at room temperature in the range from 18 to 120° using a scanning method with a step $|\Delta(2\theta)| = 0.02°$ and the counting time 10 s. Lattice parameters were calculated from the scans ($|\Delta(2\theta)| = 0.01°$, counting time 10 s) of selected Bragg reflections: (100), (110), (111), (200), (220), (211) and (310). The intensity, full width at half maximum (FWHM) and position of every measured line were fitted using the least square method by means of the X-ray Reflection Profiler computer program written by A Kachel [33].

The XPS spectra were obtained using a PHI 5700/660 Physical Electronics Photoelectron Spectrometer with monochromatized Al Kα x-ray radiation (1486.6 eV). The hemispherical mirror analyser measured the energy of the electrons with an energy resolution of about 0.3 eV. The photoelectron emission from a surface area of 800 μm $\times$ 2000 μm was recorded. All measurements were performed on a crystal broken under UHV conditions, 10^{-8} Pa.

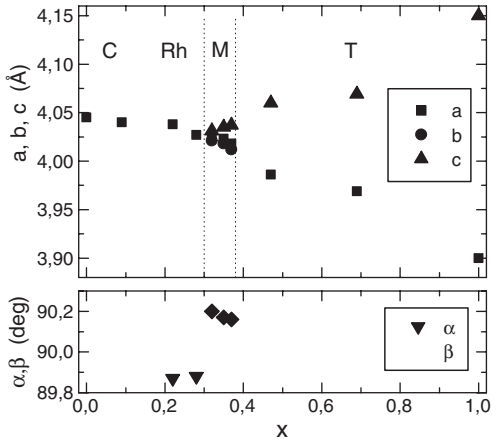

Figure 1. The room-temperature lattice parameters of $(1-x)$PMN–xPT single crystals. C, Rh, M and T denote cubic, rhombohedral, monoclinic and tetragonal symmetry, respectively.

$(1-x)$PMN–xPT crystals with x equal to 0, 0.22, 0.28, 0.32, 0.37, 0.47, 0.69 and 1 were investigated. In every case the neutralizer was used because of a charge effect which occurs for non-conducting samples. The binding energy was determined by reference to the C 1s component set. Each peak of the recorded spectrum is characteristic for a certain electron energy level of the measured elements. However, the measured binding energies are not absolutely constant but depend on the chemical environments, where functional groups are located due to modification of the valence electron distribution. These differences in relation to pure elements in the electron binding energies are called chemical shifts.

For many XPS investigations it is important to determine the relative concentrations of the various constituents. The Multipak Physical Electronics program enables quantification of the XPS spectra utilizing peak area and a peak height sensitivity factor. The standard atomic concentration calculation provides the ratio of each component to the sum of all elements, taken into account in the data. Only those elements for which the specific line is clearly visible in the spectrum are considered. For these lines the Shirley background individually selected in the region limited to the particular line is subtracted and after that integration of the peak area is performed [34]. Gaussian–Lorenzian functions were used to fit the XPS core level spectra.

3. Results and discussion

3.1. X-ray results

X-ray diffraction studies showed that all investigated crystals are single phase, of perovskite structure. The evolution of the symmetry and lattice parameters, determined at room temperature, as a function of Ti concentration is shown in figure 1. With increasing Ti concentration the symmetry changes from pseudo-cubic for PMN to rhombohedral and to monoclinic, when the concentration of the MPB ($0.32 \leqslant x \leqslant 0.37$) is achieved. For higher Ti content the symmetry is tetragonal. This indicates that our x-ray results confirm the well-described behaviour of the PMN–PT system [21]. For each Bragg reflection the full width at half maximum (FWHM) of the single component was also determined. The Ti concentration dependence of the FWHM is shown in figure 5 together with the XPS results.

Table 1. The atomic concentrations determined from XPS data obtained for different points of the $(1-x)$PMN–xPT single crystals.

		Atomic concentration (%)				
Sample		Pb	Mg	Nb	Ti	O
PMN	Nominal	**20.00**	**6.67**	**13.33**	—	**60.00**
	Real	21.75	4.61	12.18	—	61.45
		18.94	2.97	15.49	—	62.60
0.78PMN–0.22PT	Nominal	**20.00**	**5.20**	**10.40**	**4.40**	**60.00**
	Real	21.68	7.33	9.54	1.80	59.65
		21.84	2.75	10.16	4.30	60.95
0.72PMN–0.28PT	Nominal	**20.00**	**4.80**	**9.60**	**5.60**	**60.00**
	Real	19.98	0.44	12.08	5.85	61.65
		18.70	0.66	12.03	4.16	64.45
0.63PMN–0.37PT	Nominal	**20.00**	**4.20**	**8.40**	**7.40**	**60.00**
	Real	20.93	2.99	9.28	4.95	61.85
		21.75	0.89	9.81	4.76	62.79
0.53PMN–0.47PT	Nominal	**20.00**	**3.53**	**7.07**	**9.40**	**60.00**
	Real	16.77	1.26	7.98	9.67	64.32
		18.21	1.58	7.77	11.34	61.11
0.31PMN–0.69PT	Nominal	**20.00**	**2.07**	**4.13**	**13.80**	**60.00**
	Real	18.38	0.63	7.76	12.66	60.57
		20.44	1.78	5.98	11.25	60.55
PT	Nominal	**20.00**	—	—	**20.00**	**60.00**
	Real	21.18	—	—	17.39	61.43

3.2. Photoemission results

The performed XPS studies allowed us to determine the chemical composition of $(1-x)$PMN–xPT single crystals. The chemical compositions were determined for each sample at several points, and they are collected in table 1. The concentration of particular ions changes from point to point, which is essential for relaxor properties [1]. The XPS results obtained by Parmigniani *et al* [29] exhibit a random distribution of Nb and Mg ions on the cationic site. An excess of lead was observed in PT by Leinen *et al* [35] and by Preston *et al* [36]. They conclude that this excess really improved the quality of crystals. The crystal compositions determined from XPS and EDS [32] studies are in good agreement.

Figure 2 presents two survey spectra taken from the 0.78PMN–0.22PT and $PbTiO_3$ crystals. The spectra reveal the dominant peaks from the Pb, Mg, Nb, Ti and O ions along with a C 1s peak coming from carbon contamination. The high-resolution C 1s spectra of most investigated crystals showed that they consist of three components, which can be attributed to hydrocarbon (C–H) and C–C species at 284.6 eV, carboxide (C–O) at 285.9 eV and carboxylate (COO) at 287.9 eV [37]. The presence of the C 1s peak even for the surface of crystals cleft in vacuum may indicate that cleavage happens along micro-cracks, which are already contaminated by carbon compounds in the etching process and during exposure to the atmosphere. The micro-cracks were observed for some PMN–PT single crystals using an optical microscope. They may appear as an effect of thermal stress during cooling from the crystallization temperature. Also an enhanced amount of oxygen in comparison with the nominal value indicates that some of the oxygen comes from the same source as the carbon contamination. In perovskites, due to the oxygen vacancies, a rather lower amount of oxygen than nominal is observed [38].

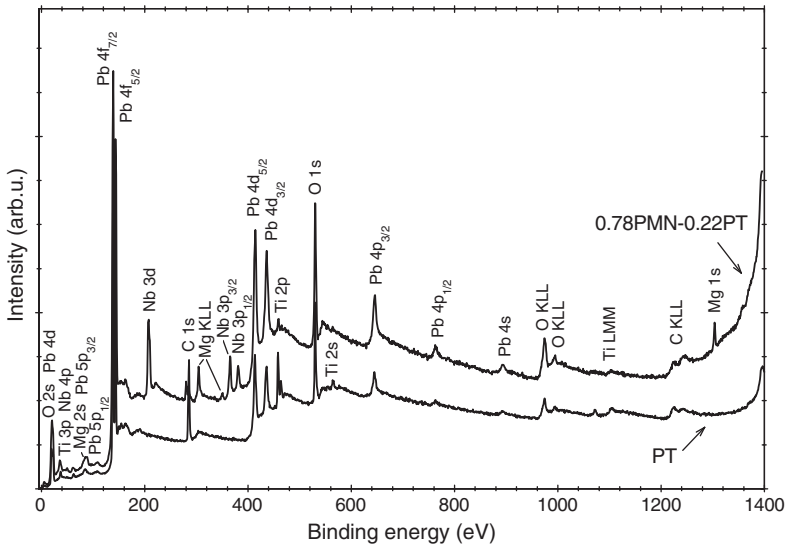

Figure 2. The survey XPS spectra of 0.78PMN–0.22PT and PT single crystals.

High-resolution spectra of the Pb 4f, O 1s, Nb 3d and Ti 2p states in the PMN–PT crystals are shown in figures 3 and 4. Because of their small intensity the Mg spectra are not involved. As is clearly seen, for all crystal compositions the Ti 2p and Nb 3d spectra consist of two peaks corresponding to their angular momentum of electrons. Only one spin–orbit doublet is observed for these elements. This means that the Ti and Nb ions exhibit only one chemical state. The binding energies of these elements are not strongly dependent on composition and they are approximately Ti $2p_{3/2} = 458$ eV, Ti $2p_{1/2} = 464$ eV, Nb $3d_{5/2} = 206.5$ eV and Nb $3d_{3/2} = 209.5$ eV. In contrast, for most of the compositions, the Pb and O spectra are not observed as one component Pb 4f spin–orbit doublet and O 1s singlet.

The Pb spectra of PMN, 0.78PMN–0.22PT, 0.72PMN–0.28PT and 0.63PMN–0.37PT crystals may be decomposed into two sets of the spin–orbit doublets, the main and the satellite S_{Pb1}. This indicates that the binding energy for the satellite line is about 137 eV (Pb $4f_{7/2}$) and 142 eV (Pb $4f_{5/2}$), and for the main line is about 138 eV (Pb $4f_{7/2}$) and 143 eV (Pb $4f_{5/2}$). The binding energy difference between each spin–orbit doublet is the same and equals 5 eV. The satellite S_{Pb1} doublet downward shift of about 1 eV from the main Pb lattice peak may be associated with the surface Pb metallic state. The Pb metal may appear as a result of the reduction of Pb^{2+} ions to Pb^0 during etching in the acetic acid. Similar sets of two Pb 4f doublets were observed for PMN and PZT thin films [30, 31, 37–40]. These four samples are fragile and micro-cracks during the cooling from crystallization process might be formed. This splitting of the Pb lines can be also explained by structural disorder characteristic for these materials and will be considered further.

The Pb 4f spectra of 0.53PMN–0.47PT and 0.31PMN–0.69PT are observed as one spin–orbit doublet and thus attributed to the lattice Pb state. The Pb 4f spectrum of $PbTiO_3$ again exhibits two binding energy states: the main peak at Pb $4f_{7/2} = 138$ eV and Pb $4f_{5/2} = 143$ eV, and the satellite S_{Pb2} at Pb $4f_{7/2} = 139$ eV and Pb $4f_{5/2} = 144$ eV. In this case, the binding energies of the additional satellite peaks are shifted towards higher values. The observed binding energy shift is about 1 eV, which can indicate that this additional state may be related to Pb^{4+}. The crystals were grown from a solvent containing Pb_3O_4 and some amount of Pb^{4+} could be built into crystals and replace the Ti ions.

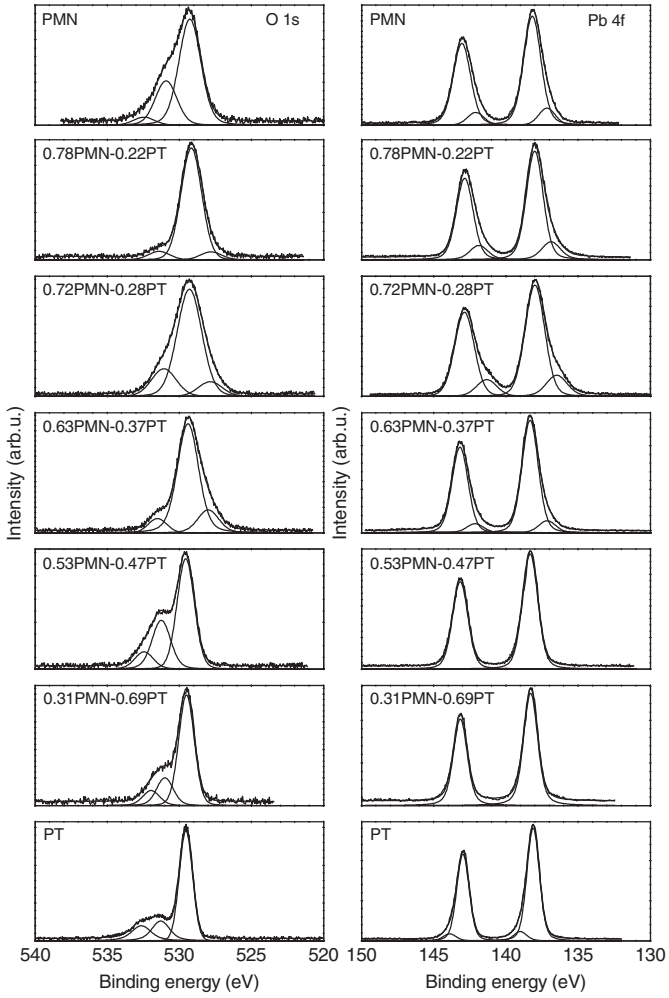

Figure 3. The high-resolution XPS spectra of the O 1s and Pb 4f photoelectrons for $(1-x)$PMN–xPT single crystals.

The nominally single O 1s peak can be decomposed into the main peak and three S_{O1}, S_{O2} and S_{O3} satellites. The spectra of PMN, 0.53PMN–0.47PT, 0.31PMN–0.69PT and PT consist of three components with binding energies of approximately: a main line at about 529.5 eV, S_{O2} at 531.5 eV and S_{O3} at 532.5 eV. The main line can be attributed to the lattice oxygen. Two further satellites S_{O2} and S_{O3} are most probably the surface components. The binding energy of the S_{O2} component is 531.5 eV and the shift from the main peak is about 2 eV. This component appears likely due to the adsorbed O atoms [29, 37, 39, 40]. The binding energy of the S_{O3} satellite is about 532.5 eV and the shift from the main peak is 3 eV. According to the literature data, we can attribute this component to adsorbed OH, CO and CO_2 [39, 40]. In spectra of 0.78PMN–0.22PT, 0.72PMN–0.28PT and 0.63PMN–0.37PT additionally to the main peak at about 529.3 eV two satellites S_{O1} and S_{O2} with binding energies of 528 and 531.5 eV, respectively, appear. As for other compositions, the S_{O2} satellite appears due to the absorbed oxygen. However, the origin of the S_{O1} component cannot be predicted with certainty. If we consider this component as a new chemical state, the assumption that oxygen

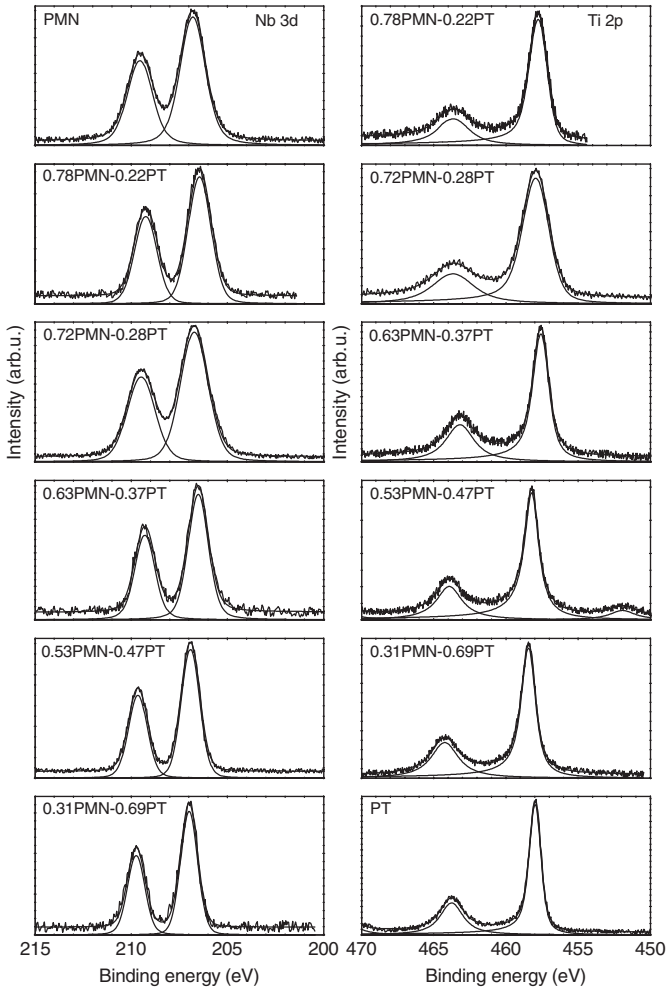

Figure 4. The high-resolution XPS spectra of the Nb 3d and Ti 2p photoelectrons for $(1-x)$PMN–xPT single crystals.

exists in another state is not very probable. Another explanation may be proposed. The S_{O1} component appears as an asymmetric broadening of the low-energy side of the main peak and therefore one can connect it with structural disorder. Similar behaviour was observed in other perovskites exhibiting the presence of disordered or amorphous phase [38].

The high-resolution Pb, Nb, Ti and O spectra show that the bulk of the $(1-x)$PMN–xPT crystals, except $PbTiO_3$, is characterized by only one chemical state for each element. Only one value of the binding energy was found. For $PbTiO_3$ crystals two Pb^{2+} and Pb^{4+} chemical states were detected. The values of binding energy of the main lines and the related chemical shifts from the atomic catalogue states for each element determined for all compositions are listed in table 2. For all compounds similar chemical shifts are observed.

The changes of the lattice components of all core-level spectra shown in figures 3 and 4 point to the regular concentration dependence of the full width at half maximum (FWHM). Figure 5 shows the dependences of the FWHM of Pb, Ti, Nb and O main peaks versus Ti content. With Ti concentration increasing, the FWHMs slightly decrease for $x = 0.22$, reach the

Table 2. The binding energies and chemical shits of the main and satellite Pb $4f_{7/2}$, Nb $3d_{5/2}$, Ti $2p_{3/2}$, O 1s XPS lines of $(1-x)$PMN–xPT single crystals. (M—main line; S_1–S_3 satellite lines, EB_M—binding energy of the main line (experiment), EB_C—binding energy (catalogue position)).

PMN							
Binding energy	Pb $4f_{7/2}$		Nb $3d_{5/2}$	Ti $2p_{3/2}$		O 1s	
(catalogue value)	136.9 eV		202.4 eV	454.1 eV		531 eV	
EB (eV)	M	S_{Pb1}	M	M	M	S_{O2}	S_{O3}
(compound)	138.2	137.1	206.8	—	529.3	530.9	532.4
Δ (eV)							
Chemical shift	+1.3		+4.4	—		−1.7	
$(\Delta = EB_M - EB_C)$							
0.78PMN–0.22PT							
Binding energy	Pb $4f_{7/2}$		Nb $3d_{5/2}$	Ti $2p_{3/2}$		O 1s	
(catalogue value)	136.9 eV		202.4 eV	454.1 eV		531 eV	
EB (eV)	M	S_{Pb1}	M	M	M	S_{O1}	S_{O2}
(compound)	138.0	136.9	206.5	457.7	529.2	527.8	531.4
Δ (eV)							
Chemical shift	+1.1		+4.1	+3.6		−1.8	
$(\Delta = EB_M - EB_C)$							
0.72PMN–0.28PT							
Binding energy	Pb $4f_{7/2}$		Nb $3d_{5/2}$	Ti $2p_{3/2}$		O 1s	
(catalogue value)	136.9 eV		202.4 eV	454.1 eV		531 eV	
EB (eV)	M	S_{Pb1}	M	M	M	S_{O1}	S_{O2}
(compound)	138.0	136.5	206.7	458.0	529.3	527.9	531.1
Δ (eV)							
Chemical shift	+1.1		+4.3	+3.9		−1.7	
$(\Delta = EB_M - EB_C)$							
0.63PMN–0.37PT							
Binding energy	Pb $4f_{7/2}$		Nb $3d_{5/2}$	Ti $2p_{3/2}$		O 1s	
(catalogue value)	136.9 eV		202.4 eV	454.1 eV		531 eV	
EB (eV)	M	S_{Pb1}	M	M	M	S_{O1}	S_{O2}
(compound)	138.3	137.1	206.5	457.6	529.4	528.0	531.5
Δ (eV)							
Chemical shift	+1.4		+4.1	+3.5		−1.6	
$(\Delta = EB_M - EB_C)$							
0.53PMN–0.47PT							
Binding energy	Pb $4f_{7/2}$		Nb $3d_{5/2}$	Ti $2p_{3/2}$		O 1s	
(catalogue value)	136.9 eV		202.4 eV	454.1 eV		531 eV	
EB (eV)	M	S	M	M	M	S_{O2}	S_{O3}
(compound)	138.3	—	206.9	458.2	529.5	531.2	532.4
Δ (eV)							
Chemical shift	+1.4		+4.5	+4.1		−1.5	
$(\Delta = EB_M - EB_C)$							
0.31PMN–0.69PT							
Binding energy	Pb $4f_{7/2}$		Nb $3d_{5/2}$	Ti $2p_{3/2}$		O 1s	
(catalogue value)	136.9 eV		202.4 eV	454.1 eV		531 eV	
EB (eV)	M	S	M	M	M	S_{O2}	S_{O3}
(compound)	138.3	—	207	458.4	529.5	531.0	532.0

Table 2. (Continued.)

Δ (eV)							
Chemical shift ($\Delta = EB_M - EB_C$)		+1.4	+4.6	+4.3		−1.5	
PT							
Binding energy		Pb $4f_{7/2}$	Nb $3d_{5/2}$	Ti $2p_{3/2}$		O 1s	
(catalogue value)		136.9 eV	202.4 eV	454.1 eV		531 eV	
EB (eV)	M	S_{Pb2}	—	M	M	S_{O2}	S_{O3}
(compound)	138.1	139.0		458.0	529.5	531.3	532.6
Δ (eV)							
Chemical shift ($\Delta = EB_M - EB_C$)		+1.2	—	+3.9		−1.5	

maxima near $x = 0.28$, then rapidly decrease up to $x = 0.47$ and then further decrease slowly. The smallest FWHM values are observed for pure $PbTiO_3$, and the biggest for crystals of composition close to the morphotropic phase boundary. In the studied $(1-x)$PMN–xPT series $PbTiO_3$ is the most ordered compound and its FWHM values may be assumed as the reference ones. The significant increases of FWHMs with Ti concentration decrease, from 1.1 eV for PT to about 2.2 eV for 0.63PMN–0.37PT, points to disorder as an origin of the core-level line broadening. Similar broadening of the x-ray photoelectron lines was found in disordered metallic alloys like CuPd [41], CuZn [26], AgPd [42], $x Nd_2O_3$–$(1-x)(3Bi_2O_3^*PbO)$ glasses [43] and $Gd_2(Ti_{1-x}Zr_x)_2O_7$ complex oxides [27].

The most experimentally evidenced broadening of the core-level lines caused by disorder was found in metallic alloys. In CuPd alloys this broadening was 0.26 eV [41]. This effect was explained by first-principles calculations [44] and within the framework of a correlated charge model [26, 45]. In both cases a Gaussian distribution of lattice site potential was shown.

The investigated PMN–PT system belongs to the class of ionic–covalent materials, with mostly ionic nature of the chemical bonds. Therefore, an greater influence of the compositional disorder on the lattice site potential than in metallic alloys is expected. In the class of ferroelectric relaxors the random distribution of the B ions (Mg, Nb and Ti in our case) is a source of random electric fields, which prevent the appearance of a long-range ferroelectric state and play an essential role in relaxor physics [18, 46–48]. The lattice site potential depends strongly on the site's chemical surroundings and should exhibit some distribution around the average value. As was stated in the introduction, the core-level spectra are sensitive to the lattice site potential and hence their broadening ought to reflect the lattice site potential distribution. Coulomb interactions are long ranged, but in the first approximation we can consider only two shells of the nearest neighbours. In addition, only these B ions contribute to random fields, whose valence differs from +4. Let us consider only the oxygen site in cubic perovskite on the basis of these assumptions. Every O ion is surrounded by two B ions at distance $0.5a$, and four Pb and eight O ions at distance $0.7a$, where a is the lattice constant. The lowest and the highest O site potentials occur when O ion is surrounded only by Mg^{2+} or by Nb^{5+} ions, respectively.

In random binary $A_{1-x}B_x$ alloys the highest disorder is expected for composition with $x = 0.5$ [47]. In our case, the $(1-x)PbMg_{1/3}Nb_{2/3}O_3$–$xPbTiO_3$ solid solutions are built from disordered $PbMg_{1/3}Nb_{2/3}O_3$ and ordered $PbTiO_3$. We believe that the highest disorder should appear for x smaller than 0.5. The influence of structural disorder, like the appearance of polar nanoregions and coexistence of phases of different symmetry, on the core-level line broadening must be also taken into account. The biggest structural disorder in the PMN–PT system is observed near the morphotropic phase boundary. The FWHMs of XPS spectra reach maximum

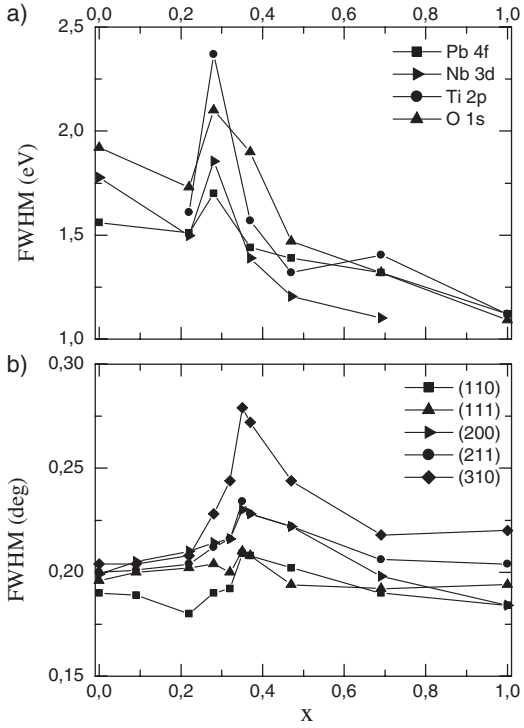

Figure 5. The FWHM of XPS lines (a) and Bragg's reflections (b) $(1-x)$PMN–xPT single crystals versus Ti concentration.

values for compositions close to the MPB (figure 5(a)). Also the FWHMs of the Bragg's reflections show similar concentration behaviour, with maxima near the MPB (figure 5(b)).

We would like to stress here that another possible reason for the core-level line broadening, such as imperfections of sample surface and charging of sample during experiment, should also be consider. Moreover, the FWHM values of the Bragg's reflections determined from powders do not give information of the highest reliability since their values can be affected by instrumental conditions, the size of coherently scattering domains and microstrains. The size of crystallites can cause broadening of the diffraction lines only for grains smaller than 10^{-5} m, while strain can be reduced by suitable annealing of sample. The powders used have grain size bigger than this limit. Our room-temperature diffraction patterns were recorded for unannealed samples because of the risk of chemical decomposition at high temperatures. It must be pointed out that the room-temperature diffraction patterns recorded after high-temperature measurements show the same values of the FWHMs of Bragg reflections. These two features indicate that both grain size and strain should be excluded as reasons for the observed Bragg's reflection broadening. Moreover, the regular concentration evolutions of FWHMs of XPS and x-ray lines allow us to believe that observed line broadening originates from structural disorder.

4. Conclusions

PMN–PT single crystals from the whole concentration range were investigated by x-ray diffraction and x-ray photoelectron spectroscopy. Our room-temperature x-ray results are

consistent with the well-described behaviour of the PMN–PT system [21]. Pure PMN possesses pseudo-cubic symmetry which with increasing Ti content transforms into rhombohedral, then to monoclinic in the vicinity of the morphotropic phase boundary and finally to tetragonal, characteristic for $PbTiO_3$.

High-resolution core-level spectra of the Pb 4f, O 1s, Nb 3d and Ti 2p were studied. For all crystal compositions in the case of the Ti 2p and Nb 3d spectra only one spin–orbit doublet is observed, which suggests that these elements exhibit only one chemical state. In contrast, for most of the compositions, the Pb and O spectra may be decomposed into two sets of spin–orbit doublets and three singlets, respectively. The main lines are connected with the lattice while the satellite ones may be associated with surface states. The high-resolution core-level spectra of the Pb 4f, O 1s, Nb 3d and Ti 2p states show that the bulk of the PMN–PT crystals is characterized by only one chemical state for each element except $PbTiO_3$, for which Pb^{2+} and Pb^{4+} states were detected.

The evolution of the lattice components of all core-level spectra points to regular concentration dependence of the full width at half maximum. With Ti content increasing, FWHMs slightly decrease for $x = 0.22$, reach the maxima near $x = 0.28$, then rapidly decrease up to $x = 0.47$ and then further decrease slowly. The smallest FWHM values are observed for pure $PbTiO_3$, while the biggest are for crystals of composition close to the morphotropic phase boundary. The explanation of this broadening of the core-level lines is directly related to the disorder and can be well interpreted within the framework of the random field model. The investigated PMN–PT system belongs to the class of ionic–covalent materials; therefore, a large influence of the compositional disorder on the lattice site potential is expected. In the class of ferroelectric relaxors the random distribution of the B ions is a source of random electric fields which prevent the appearance of a long-range ferroelectric state and play an essential role in relaxor physics [18, 46–48]. The lattice site potential depends strongly on the site's chemical surroundings and should exhibit some distribution around the average value. Also the FWHM of the Bragg's reflections show similar concentration behaviour with maxima near the MPB. Our complementary XPS and x-ray diffraction studies showed that in the $PbMg_{1/3}Nb_{2/3}O_3$–$PbTiO_3$ system the highest disorder appears near the morphotropic phase boundary.

References

[1] Cross L E 1987 *Ferroelectrics* **76** 241
[2] Kuwata J, Uchino K and Nomura S 1982 *Japan. J. Appl. Phys.* 1 **21** 1298
[3] Park S-E and Shrout T R 1997 *J. Appl. Phys.* **82** 1804
[4] Bonneau P, Garnier P, Calvarin G, Husson E, Gavarri J R, Heiwat A W and Morell A 1991 *J. Solid State Chem.* **91** 350
[5] Takesue N, Fujii Y and You H 2001 *Phys. Rev.* B **64** 184112
[6] You H and Zhang Q M 1997 *Phys. Rev. Lett.* **79** 3950
[7] Fanning D M, Robinson I K, Young S T, Colla E V, Viehland D D and Payne D A 2000 *J. Appl. Phys.* **87** 840
[8] Xu G, Shirane G, Copley J R D and Gehring P M 2004 *Phys. Rev.* B **69** 064112
[9] Hirota K, Ye Z-G, Wakimoto S, Gehring P M and Shirane G 2002 *Phys. Rev.* B **65** 104105
[10] Chen J, Chan H M and Harmer M P 1989 *J. Am. Ceram. Soc.* **72** 593
[11] Yan Y, Pennycook S J, Xu Z and Viehland D 1998 *Appl. Phys. Lett.* **72** 3145
[12] Prouzet E, Husson E, de Mathan N and Morell A 1993 *J. Phys.: Condens. Matter* **5** 4889
[13] Blinc R, Gregorovic A, Zalar B, Pirc R, Laguta V V and Glinchuk M D 2000 *Phys. Rev.* B **63** 024104
[14] Wakimoto S, Stock C, Ye Z-G, Chen W, Gehring P M and Shirane G 2002 *Phys. Rev.* B **66** 224102
[15] Dkhil B, Kiat J M, Calvarin G, Baldinozzi G, Vakrushev S B and Suard E 2001 *Phys. Rev.* B **65** 024104
[16] Vakrushev S, Zhukov S, Fetisov G and Chernyshov V 1994 *J. Phys.: Condens. Matter* **6** 4021
[17] de Mathan N, Husson E, Calvarin G, Gavarri J R, Hewat A W and Morell A 1991 *J. Phys.: Condens. Matter* **3** 8159

[18] Pirc R and Blinc R 1999 *Phys. Rev.* B **60** 13470
[19] Ye Z-G and Schmid H 1993 *Ferroelectrics* **145** 83
[20] Ye Z-G, Bing Y, Gao J, Bokov A A, Stephens P, Noheda B and Shirane G 2003 *Phys. Rev.* B **67** 104104
[21] Noheda B, Cox D E, Shirane G, Ye Z-G and Gao J 2002 *Phys. Rev.* B **66** 054104
[22] Singh A K and Pandey D 1999 *J. Phys.: Condens. Matter* **13** L931
[23] Viehland D and Li J F 2002 *J. Appl. Phys.* **92** 7690
[24] Davis M, Damianovic D and Setter N 2005 *J. Appl. Phys.* **97** 064101
[25] Cole R J, Brooks N J and Weightman P 1997 *Phys. Rev. Lett.* **78** 3777
[26] Lewis D, Cole R J and Weightman P 1999 *J. Phys.: Condens. Matter* **11** 8431
[27] Chen J, Lian J, Wang L N, Ewing R C, Wand R G and Pan W 2002 *Phys. Rev. Lett.* **88** 105901
[28] Nachimuthu P, Thevuthasan S, Engelhard N H, Weber W J, Shuh D K, Hamdan N M, Mun B S, Adams E M, McCready D E, Shutthanandam V, Lindle D W, Balakrishnan G, Paul D M, Gullikson E M, Perera R C C, Lian J, Wang L M and Ewing R C 2004 *Phys. Rev.* B **70** 100101
[29] Parmigiani F, Rollandi L, Samoggia G and Depero L E 1996 *Solid State Commun.* **100** 801
[30] Gupta S M, Kulkarni A R, Vedpathak M and Kulkarni S K 1996 *Mater. Sci. Eng.* B **39** 34
[31] Cao J L, Li L T, Wang Y L, Zhao J Q and Gui Z L 2001 *Mater. Res. Bull.* **36** 2103
[32] Kania A, Słodczyk A and Ujma Z 2005 *J. Cryst. Growth* submitted
[33] Kachel A 1992 *X-ray Profiler,* version 2.0
[34] Moulder J F, Stickle W F, Sobol P E and Bomben K D 1995 *Handbook of X-ray Photoelectron Spectroscopy Physical Electronics* Physical Electronics, Inc.
[35] Leinen D, Caballero A, Fernandez A, Espinos J P, Justo A, Gonzalez-Elipe A R, Martin J M and Maurin-Perrier B 1996 *Thin Solid Films* **272** 99
[36] Preston K D and Haertling G H 1992 *Proc. 9th Int. Symp. Appl. Ferroelectrics* (Piscataway, NJ: IEEE) p 23
[37] Zhu T J and Lu L 2004 *J. Appl. Phys.* **95** 241
[38] Talik E, Kruczek M, Sakowska H, Ujma Z, Gała M and Neumann M 2004 *J. Alloys Compounds* **377** 259
[39] Takatani S, Miki H, Kushida-Abdelghafar K and Torii K 1999 *J. Appl. Phys.* **85** 7784
[40] Wakiya N, Kuroyanagi K, Ksuan Y, Shinozaki K and Mizutani N 2000 *Thin Solid Films* **372** 156
[41] Cole R J, Brooks N J and Weightman P 1997 *Phys. Rev. Lett.* **78** 3777
[42] Newton A W, Haines S, Weightman P and Cole R J 2004 *J. Electron Spectrosc. Relat. Phenom.* **136** 235
[43] Culen E, Pop L, Simon V, Meumann M and Btatu I 2004 *J. Non-Cryst. Solids* **337** 62
[44] Faulkner J S, Wang Y and Stockes G M 1998 *Phys. Rev. Lett.* **81** 1905
[45] Magri R, Wei S-H and Zunger A 1990 *Phys. Rev.* B **42** 11388
[46] Westpal V, Kleemann W and Glinchuk M D 1992 *Phys. Rev. Lett.* **68** 847
[47] Glinchuk M D and Farhi R 1996 *J. Phys.: Condens. Matter* **8** 6985
[48] Kleemann W, Samara G A and Dec J 2005 *Polar Oxides: Properties, Characterisation and Imaging* ed R Waser, U Böttger and S Tiedke (Weinheim: WILLRY-VGH Verlag & Co KGaA)